Materials Research Bulletin 60 (2014) 313–321

Contents lists available at ScienceDirect

Materials Research Bulletin

journal homepage: www.elsevier.com/locate/matresbu

Characterization of ZnS thin films synthesized through a non-toxic precursors chemical bath

C.A. Rodríguez [a], M.G. Sandoval-Paz [b], G. Cabello [c], M. Flores [d], H. Fernández [d], C. Carrasco [a,*]

[a] Department of Materials Engineering, Faculty of Engineering, University of Concepción, Edmundo Larenas 270, Concepción 4070409, Chile
[b] Department of Physics, Faculty of Physics and Mathematics, University of Concepción, Concepción, Chile
[c] Department of Basic Sciences, Faculty of Sciences, University of Bío-Bío, Campus Fernando May, Chillán, Chile
[d] Department of Physics, Faculty of Physics and Mathematics, University of Chile, Beauchef 850, Santiago, Chile

ARTICLE INFO

Article history:
Received 14 March 2014
Received in revised form 11 August 2014
Accepted 30 August 2014
Available online 2 September 2014

Keywords:
A. Thin films
A. Semiconductors
B. Chemical synthesis
B. Optical properties
C. X-ray diffraction

ABSTRACT

In solar cells, ZnS window layer deposited by chemical bath technique can reach the highest conversion efficiency; however, precursors used in the process normally are materials highly volatile, toxic and harmful to the environment and health (typically ammonia and hydrazine). In this work the characterization of ZnS thin films deposited by chemical bath in a non-toxic alkaline solution is reported. The effect of deposition technique (growth in several times) on the properties of the ZnS thin film was studied. The films exhibited a high percentage of optical transmission (greater than 80%); as the deposition time increased a decreasing in the band gap values from 3.83 eV to 3.71 eV was observed. From chemical analysis, the presence of ZnS and $Zn(OH)_2$ was identified and X-ray diffraction patterns exhibited a clear peak corresponding to ZnS hexagonal phase (1 0 3) plane, which was confirmed by electron diffraction patterns. From morphological studies, compact samples with well-defined particles, low roughness, homogeneous and pinhole-free in the surface were observed. From obtained results, it is evident that deposits of ZnS–CBD using a non-toxic solution are suitable as window layer for TFSC.

1. Introduction

Chemical bath deposition (CBD) has been used along numerous years to deposit metal-chalcogenide semiconductor thin films. CBD method constitutes a technique relatively fast, easy and inexpensive – it works at low temperature and low atmospheric pressure – which can be easily employed at industrial scale. Through this method, a growth of semiconductor thin films is performed on solid substrates immersed in a solution containing a source of metallic cations, one or more complexing agents and a source of anions. The chemical reactions in the solution give rise to compound formation, thus the basis for this technique is its controlled precipitation. Among other deposition techniques such as thermal evaporation [1], sputtering [2], photochemical deposition (PCD) [3], and others, CBD is one of the most suitable methods to deposit semiconductor thin films for solar cell applications. However, the deposition of ZnS thin films by CBD technique is characterized by a slow growth rate when compared with those other techniques. Whereas for thermal evaporation and PCD the typical growth rate reached is around 1 μm/h, to obtain layers greater than 100 nm/h for CBD gets complicated. Depending on the deposition conditions the growth rate can be increased, but always below 70 nm/h [4]. Nonetheless, for solar cells application the thickness of windows layer must be maintained close to 100 nm to prevent further absorption of the light. Hence CBD is a technique industrially feasible and, still more; CBD is one of the most suitable techniques to deposit semiconductors thin films for solar cells applications.

Currently, 20.3% is the best conversion efficiency rate for thin-film solar cells (TFSC) based on $Cu(In,Ga)Se_2$ (CIGS) that modern technology has achieved so far using a window layer of CdS grown by means of CBD (CdS–CBD) [5]. However, the relatively low band gap of CdS (2.42 eV) means that light with wavelengths lower than 520 nm is not transmitted to the absorbent layer (lower blue response), and thence, the quantum efficiency of the devices is reduced [6,7]. At the same time, CdS–CBD produces serious environmental and health problems due to the large amount of Cd-containing waste during deposition process [8,9]. Similar efforts should also be focused on manufacturing Cd-free TFSC.

* Corresponding author. Tel.: +56 41 2207181.
E-mail address: ccarrascoc@udec.cl (C. Carrasco).

http://dx.doi.org/10.1016/j.materresbull.2014.08.047
0025-5408/

Several materials have been investigated as window layer, such as ZnS, In_2S_3, ZnSe, $Zn(S_xSe_{1-x})$, SnS, and $Zn_xIn_{1-x}Se$ [6,10,11]. Among them, ZnS is considered the most promising window layer because CIGS thin film solar cells using a ZnS window layer deposited by CBD (ZnS–CBD) can reach the highest conversion efficiency. Besides, ZnS is less toxic and cheaper than CdS [12]. Moreover, the band gap of ZnS (3.6 eV) is wider than that of CdS (2.4 eV), which improves the short-circuit current of the solar-cell device [6], thus solving the transmission problem at wavelengths lower than 520 nm.

Growth of ZnS–CBD for its application as window layer has been reported by several authors [13–15]. Although the use of zinc reduces the contaminants' wastes due to being Cd-free, the compound's synthesis is far from being non-toxic. Commonly, the reaction solution to deposit ZnS thin films will contain the following elements: salt of Zn which gives Zn^{2+} ions, one or more complexing agents – usually ammonia (NH_4) and/or hydrazine (N_2H_4) – and thiourea (H_4N_2SC) which gives S^{2-} ions. Ammonia and hydrazine are materials highly volatile, toxic and harmful to the environment and health. Besides, the ammonia volatility changes the pH of the reaction solution and, therefore, it means that the results are irreproducible in many cases [16]. On the other hand, sodium citrate has appeared as a non-toxic complexing agent mostly used to synthesize ZnS–CBD. Agawane et al. [17] and Liu et al. [18] have reported the deposition of ZnS thin films using sodium citrate as a complexing agent; however, an ammonium hydroxide solution (NH_4OH) is added to regulate its pH, which has a risk of generating ammonia. Thus, the deposit of ZnS–CBD has at least one harmful compound that will become a major environmental problem for industrial production.

Otherwise, in order to avoid the use of harmful complexing agents, some studies report ZnS–CBD growth through acidic solutions based on using HCl to achieve pH control and thioacetamide (C_2H_5NS) as a S^{2-} ions source, then reacting in the solution and giving rise to the toxic compound $H_2S_{(g)}$ [19]. As can be seen, most of the current reports informing about ZnS–CBD growth has the use of toxic substances as a common factor.

As a contribution to avoid the use of toxic precursors, this work proposes the study of the properties of ZnS thin films grown by means of a new eco-friendly route. For the first time, a non-toxic alkaline solution containing a mixture of sodium citrate and a natural acidifying as complexing agents, potassium hydroxide as an OH^- ions source replacing ammonium hydroxide was used for the deposition. Optical, chemical, microstructural and morphological properties of ZnS thin films deposited on glass substrate through CBD using the above mentioned non-toxic solution were measured. The variation of these properties in respect to deposition time – and hence thickness – is also introduced, analyzed and compared with those reported up-to-date in literature for ZnS thin films grown from toxic solutions.

2. Experimental details

Thin films were grown on soda-lime glass substrate (25 mm × 75 mm × 1 mm) by chemical bath method from an aqueous solution containing 20 ml (0.05 M) of zinc sulfate heptahydrated (Sigma–Aldrich, 99% purity), 20 ml (0.5 M) of sodium citrate dehydrate (Sigma–Aldrich, 99% purity), 20 ml (0.025) of tartaric acid (Sigma–Aldrich, 99.5% purity) and 10 ml (0.5 M) of thiourea (Sigma–Aldrich, 99% purity). Deionized water was added to reach a volume of 100 ml and pH was adjusted to 10.5 added appropriate amounts of KOH (J.T. Baker, 88% purity) and a buffer solution pH 10.

Before deposition, the glass substrates were cleaned with water and soap, rinsed with deionized water and dried at room temperature. The cleaned substrates were vertically positioned on a beaker containing the reaction solution, which was introduced in a bath at 75 °C. After 4 h, the substrates were removed from the solution and then rinsed with deionized water. This process was done one, two, three and four times in order to obtain thicker films (i.e., multiple depositions on a single substrate or growth in several times), which correspond to samples grown at 4, 8, 12 and 16 h, respectively. Samples were dried at room temperature and then stored in a dry place. All samples obtained were colorless, translucent, reflecting and adherent to substrate.

Concerning the characterization of thin films, optical, chemical, structural and morphological properties were measured. The optical transmittance and absorbance of ZnS thin films were measured at room temperature using a spectrophotometer UV–vis PerkinElmer model Lambda 25 with 1 nm resolution. The chemical composition was studied by means of chemical binding energy of the elements through X-ray photoelectron spectroscopy technique (XPS), using an XPS–Auger PerkinElmer spectrometer model PHI 1257 which includes an ultra-high vacuum chamber, a hemispheric electron energy analyzer and an X-ray source, with Kα radiation unfiltered from an Al ($h\nu$ = 1486.6 eV) anode. The structural properties of thin films were studies through grazing angle X-ray diffraction technique using an X-ray diffractometer Bruker D8 Advance. X-ray source was Cu Kα at 40 kV and 30 mA. In order to complement XRD data, transmission electron microscopy (TEM) was performed (TEM, JEOL JSM 1200 EXII). Finally, the surface morphology was investigated by means of atomic force microscopy (AFM) using an Omicron SPM1. Surface roughness (RMS) of samples was calculated by using WSxM software [20] over $1000 \times 1000\ nm^2$ images.

3. Results and discussion

3.1. Reaction mechanism

The deposition process is based on the slow release of Zn^{2+} and S^{2-} ions in solution, which are then condensed on the substrate surface. The deposition of ZnS occurs when the ionic product of Zn^{2+} and S^{2-} exceeds the solubility product of ZnS. $ZnSO_4$ was used as the Zn^{2+} ions source and the thiourea provided S^{2-} ions by hydrolysis in an alkaline solution, according to the following reactions:

$$ZnSO_4 \rightarrow Zn^{2+} + SO_4{}^{2-} \quad (1)$$

$$KOH \rightarrow K^+ + OH^- \quad (2)$$

$$SC(NH_2)_2 + OH^- \rightarrow SH^- + CH_2N_2 + H_2O \quad (3)$$

$$SH^- + OH^- \rightarrow S^{2-} + H_2O \quad (4)$$

Hence, free Zn^{2+} ions react with free S^{2-} ions to form ZnS as follow:

$$Zn^{2+} + S^{2-} \rightarrow ZnS_{(s)} \quad (5)$$

Eq. (5) is part of the chemical bath growth mechanism called 'ion by ion mechanism' [21]. It is well known that using complexing agents is very important in CBD processes, therefore the choice of suitable agents is essential in the growth of thin films. In this work, sodium citrate (CIT) and tartaric acid (TTA) were used as complexing agents to control the slow release of Zn^{2+} ions, as follow [22,23]:

$$CIT^{3-}{}_{(ac)} + Zn^{2+}{}_{(ac)} \rightarrow [Zn(CIT)]^-{}_{(ac)} \quad (6)$$

$$TTA_{(ac)} + Zn^{2+}{}_{(ac)} \rightarrow [Zn(TTA)]_{(ac)} \quad (7)$$

Table 1
Chemical reaction and their corresponding formation and dissociation constants calculated a 25° C.

Chemical reaction	Formation or dissociation constants	Reference
$Zn^{2+} + 2OH^- \rightarrow Zn(OH)_2$	$\beta = 10^{10.08}$	[25]
$Zn^{2+} + CIT^{3-} \rightarrow Zn(CIT)^-$	$\beta = 10^{4.98}$	[26]
$Zn^{2+} + TTA \rightarrow Zn(TTA)^{2+}$	$\beta = 10^{2.68}$	[27]
$HCIT^{2-} \rightarrow CIT^{3-} + H^+$	$K = 10^{-5.69}$	[26]
$HTTA^+ \rightarrow TTA + H^+$	$K = 10^{-2.01}$	[27]

From Eqs. (4),(6) and (7), complexes and sulfide ions migrate to the substrate surface, where they react to form ZnS as follows:

$$[Zn(CIT)]^-_{(ac)} + S^{2-} \rightarrow ZnS_{(s)} + CIT^{3-}{}_{(ac)} \quad (8)$$

$$[Zn(TTA)]_{(ac)} + S^{2-} \rightarrow ZnS_{(s)} + TTA_{(ac)} \quad (9)$$

Considering "L" as the complexing agents, the complete reaction can be written as:

$$ZnL + CS(NH_2)_2 + 2OH^- \rightarrow ZnS_{(s)} + L + CH_2N_2 + 2H_2O \quad (10)$$

Presence of OH^- ions in the reaction solution made the zinc hydroxide to appear as an undesirable compound in zinc sulfide thin films grown by chemical bath method, which can be explained by the following reactions:

$$Zn^{2+} + 2OH^- \rightarrow Zn(OH)_{2(s)} \quad (11)$$

$$Zn(OH)_2 + S^{2-} \rightarrow ZnS_{(s)} + 2OH^- \quad (12)$$

Eqs. (11) and (12) correspond to the second growth mechanism known as 'cluster by cluster mechanism' [21]. The driving force of this ion exchange is the minimization of Gibbs energy due to the difference between the solubility product constant (k_{ps}) of both compounds ZnS and $Zn(OH)_2$: 10^{-24} and 10^{-16}, respectively. However, the relatively low difference between both solubility products, in one way or another, causes $Zn(OH)_2$ to be usually included in ZnS films. A good approximation for identifying the groups of intermediate chemical species that are formed during the chemical reaction can be obtained through the diagram of distribution of soluble species, having in mind that the dominant species depend strongly on the chemical reagents used in the chemical bath [24]. In the reaction solution, the Zn^{2+} ions can react with dissolved ions of OH^-, CIT^{3-} and TTA to form several soluble species, but our study becomes specifically interested in $Zn(OH)_2$, $Zn(CIT)^-$ and $Zn(TTA)^{2+}$. Table 1 shows the chemical reactions and their corresponding formation (β) and dissociation (K) constants at 25 °C as reported in the cited literature. In all cases, equilibrium constants were calculated by having in mind the concentrations in (mol l^{-1}), knowing that $[OH^-][H^+] = 10^{-14}$ (mol l^{-2}) and taking the Zn^{2+} ions as a reference. Fig. 1 shows the distribution of species, r_i, calculated as a function of the pH value by considering Zn^{2+} ion as a reference and the $[CIT^{3-}]$ and [TTA] values from experimental condition. From Fig. 1, it is observed that for pH <10.5, most of the Zn^{2+} ions are complexed by sodium citrate and, moreover, there is a very small amount of free Zn^{2+} ions, provoking $Zn(TTA)^{2+}$ concentration to be very low. In order to observe $Zn(TTA)^{2+}$ behavior, their distribution of species is inserted in Fig. 1, showing a similar trend that $Zn(CIT)^-$ as the pH rises. On the other hand, for pH >11, the $Zn(CIT)^-$ concentration diminishes considerably thus giving rise to a large increase in $Zn(OH)_2$ concentration. Then, in order to avoid the $Zn(OH)_2$ in thin films, a pH <11 should be used for the growing of the films. However, to facilitate the alkaline hydrolysis of thiourea it is necessary to maintain the pH value as high as possible. Thus, considering both conditions, the optimum pH value must be maintained between 10 and 11. For this reason,

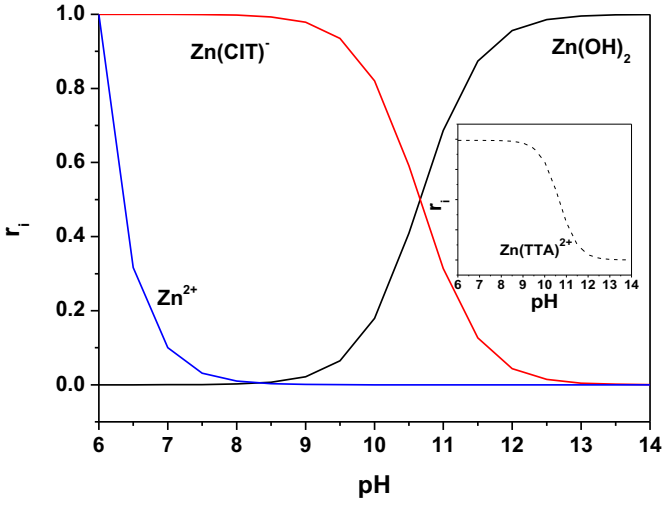

Fig. 1. Distribution diagram for soluble species for the chemical bath composed by Zn–CIT–TTA–H_2O.

10.5 was the pH used to permit an adequate hydrolysis of thiourea and, simultaneously, to avoid hydroxide precipitation as much as possible.

3.2. Optical properties

The optical properties of ZnS thin films grown on quartz substrates were taken from transmittance (T) and absorbance (A) measurements in a range of 250–850 nm. Clean quartz substrate without coating was used as a reference for optical measurements. Fig. 2(a) shows the transmittance spectra of ZnS thin films, where the absorption edges of all films were sharp and shifted toward a greater wavelength from 343 nm to 360 nm with increasing deposition time. From these spectra, it is possible to observe that all films exhibit a high optical transmission (close to 80%) in the visible range and in a part of the UV region for wavelengths greater than absorption edge, and as the deposition time increases maxima and minima of intensity appear due to the increase in the thin films thickness. As been previously reported by Refs. [28] and [29], these results indicate that films have a good homogeneity in the sharp and size of the grains, and low defect concentration in the films. G.L. Agawane et al. mentioned that thickness, uniformity and RMS values determine window layer's optical characteristics such as transmittance, absorbance and refractive index, and that the samples as revealed by high optical transmission are thin and with a slightly rough morphology, resulting in a low light dispersion in comparison to thicker and rougher samples [4]. Fig. 2(b) shows the absorbance spectra of ZnS thin films, where a low optical absorption percentage in the range of 300–850 nm can be observed, making the samples suitable as window layer material. At the same time, it is possible to observe that the region of increased absorption shifts slightly to a greater wavelengths region. This phenomenon was expected due to the increase of thin films thickness, which is characterized by the appearance of oscillations in the spectra.

The optical absorption theory in semiconductors relates the absorption coefficient α to the photon energy $h\nu$ to allow direct transitions, as follows:

$$\alpha h\nu = A^* \times (h\nu - E_g)^{1/2} \quad (13)$$

where α is the absorption coefficient, A^* constant, h Planck constant and E_g band gap energy.

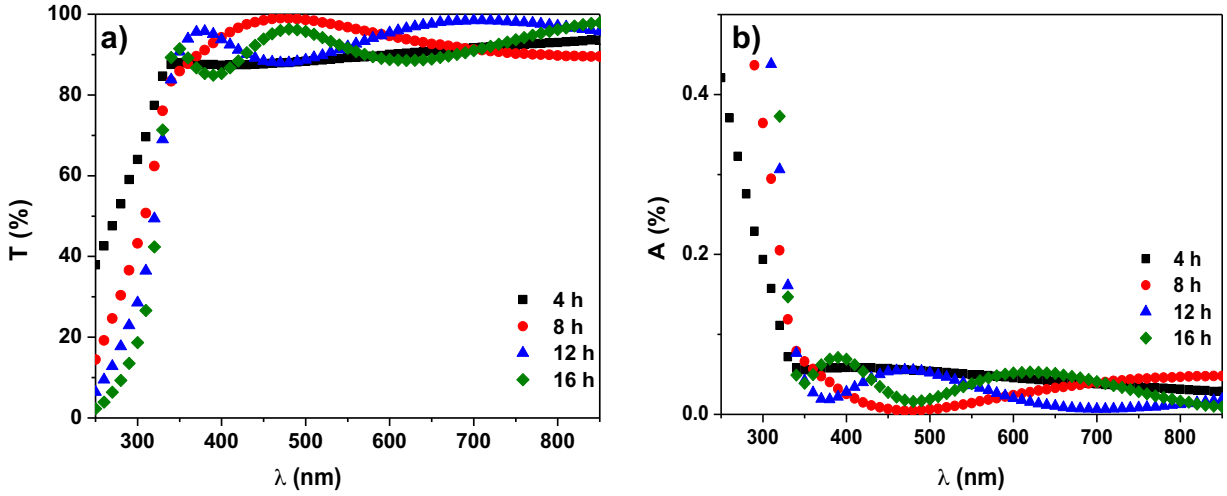

Fig. 2. (a) Transmittance and (b) absorbance spectra obtained for ZnS thin films at different deposition times.

From the transmission spectra, near the fundamental absorption edge, the values of absorption coefficient α are calculated in the region of strong absorption by using the relation:

$$\alpha = \left(\frac{1}{d}\right) \times \ln\left(\frac{1}{T}\right) \tag{14}$$

where d is the thickness and T is the transmittance. Therefore, by means of transmission spectra, it is possible to obtain the band gap of the thin films [30]. Fig. 3 shows the plots of α^2 vs. $h\nu$ for the ZnS thin films deposited at different deposition times. Extrapolation of the linear portion of the curve to $\alpha^2 = 0$ determines the band gap value, E_g. Band gap values were 3.83, 3.76, 3.73 and 3.71 eV for ZnS thin films grown at 4, 8, 12 and 16 h, respectively, where a decrease in the band gap values was present as the deposition time increased. It is evident that an increase in deposition time and consequently in the thickness of the films leads to a decrease in band gap that can be attributed to (i) the quantum confinement, because it is well known that the band gap in thin films is greater than in bulk material (for example, $E_g^{ZnS} = 3.6$ eV in bulk) [31]; however, it is expected that as thickness increases the band gap reaches asymptotically the band gap value of the bulk material

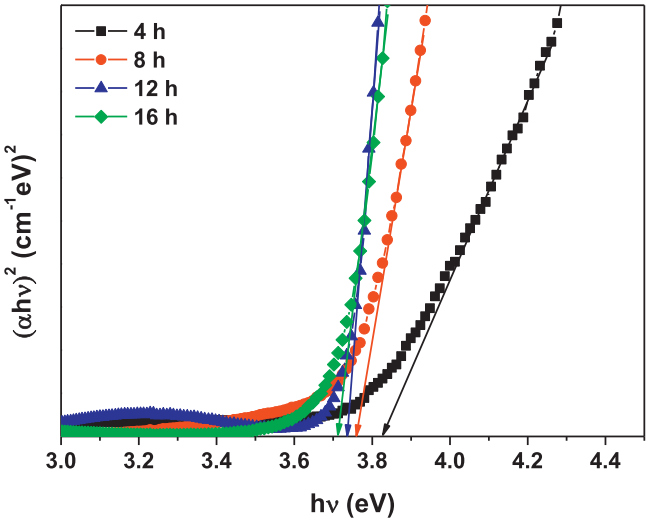

Fig. 3. Plot of $(\alpha h\nu)^2$ vs. $h\nu$ for ZnS thin films grown at 4, 8, 12 and 16 h.

caused by an increase in grain size [32]. (ii) The formation of defect during growth of the films through chemical bath has been reported by several authors [33–35] which, after the increase in thicknesses, can reduce the width of the band gap as a result of band tails [36]. It is possible to estimate the crystal size by the following equation [37]:

$$E = \frac{h^2}{4md^2} \tag{15}$$

Where E is the band gap energy difference between ZnS thin film and ZnS bulk, d is the typical crystal size, and m is the effective mass of electron ($m = 0.39\, m_0$ for ZnS, m_0: electron mass). According to Eq. (15) the crystal size are 2.96, 3.47, 3.85 and 4.18 nm for ZnS thin films deposited at 4, 8, 12 and 16 h, which indicates the nanocrystalline nature of the samples. The previous values should not be taken as absolute due to this calculation as it considers only quantum confinement effects, and probably E_g values are also modified by band tails effects. High optical transmission and wide band gap are one of the most important features for window layers application. Thus, synthesize ZnS thin films with these properties through a solution no-harmful for the environment, is an important step in the solar energy development and environmental protection.

3.3. Chemical analysis

The chemical states of the constituent elements of the thin films were determined through XPS technique. All the binding energies measured at various peaks were calibrated by the binding of C 1s (284.5 eV). Fig. 4 shows the high-resolution spectra of S 2p (Fig. 4(a)) and of Zn 2p (Fig. 4(b)) signals for ZnS thin films grown at different deposition times. The signals were fitted by two peaks at 161.6 ± 0.1 eV (3/2) and 162.8 ± 0.1 eV (1/2) binding energies, corresponding to the sulfur atoms bonded to zinc atoms (S—Zn) [15]. On the other hand, as shown in Fig. 4(b), all cases show that the Zn $2p_{3/2}$ signals consist of two peaks positioned at 1021.9 ± 0.1 eV and 1022.7 ± 0.1 eV, which can be attributed to zinc atoms bonded to hydroxide (Zn—OH) and zinc atoms bonded to sulfur atoms (Zn—S), respectively [9,15]. It is well known that in ZnS thin films grown by CBD in alkaline solution, the Zn—OH bond usually appears [9,15]. This phenomenon can be understood by reviewing the growth mechanism described by Eq. (5) for ion-by-ion mechanism, and by Eqs. (11) and (12) for cluster-by-cluster

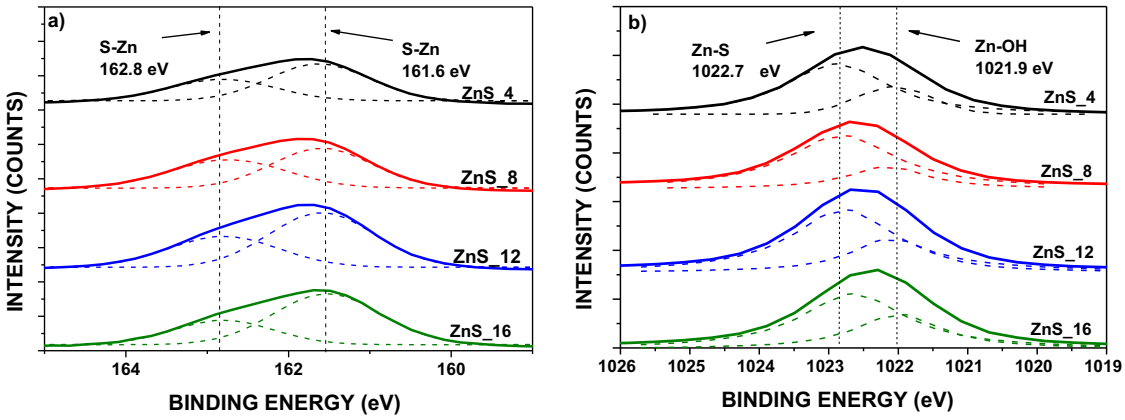

Fig. 4. High-resolution XPS spectra of (a) S 2p and (b) Zn $2p_{3/2}$ of ZnS thin films grown at different times.

mechanism. Other studies have investigated the predominance of one of these mechanisms over the other, leading to the conclusion that both participate jointly in the growth of thin films on the substrate [21]. However, it is possible to prefer one growing mechanism over the other by modifying the deposition conditions. The pH and solubility product constants play an important role, especially in ZnS–CBD thin films. In alkaline solutions, in order to promote hydrolysis of the thiourea, OH^- ions are added to the reaction solution where they inevitably react with Zn^{2+} ions to form a metastable solid phase, $Zn(OH)_2$. The greater value of the constant of solubility products of the $Zn(OH)_2$ (10^{-16}) compared with the ZnS (10^{-24}) causes that the OH^- ions to be replaced by S^{2-} ions until the phase change occurs completely [21]. This difference in values of solubility product constants between both compounds is relatively lower than that of the other water insoluble semiconductors compounds (CdS: 10^{-28}–$Cd(OH)_2$: 10^{-14}/PbS: 10^{-28}–$Pb(OH)_2$: 10^{-16}), which cause that the ionic exchange between hydroxides and sulfides during the growth of the thin films does not be completely performed in most cases.

The presence of phases different to ZnS in the studied thin films is likely to affect the films properties. However, thin-film solar cells based on CIGS using a Zn(OH,S) window layer have been reported with similar efficiencies compared to devices using a pure ZnS thin film as a window layer [6,38]. This way, according to the results reported below, we can expect that the presence of metallic hydroxide does not affect negatively the properties of the analyzed thin films.

In Fig. 4(b), it is possible to observe that the Zn $2p_{3/2}$ peaks are slightly shifted at lower binding energies as the deposition time increases, which might indicate a variation in the $Zn(OH)_2$ content in ZnS thin films. In order to achieve a better understanding of what happened inside the sample as deposition time increased, a comparative study of relative composition using the MultiPak® software was performed [39]. Method used for quantifying utilizespeak area sensitive factors and peak height sensitive factors explained in details by Wagner et al. [40], which consider a homogeneous sample in the analysis volume. As shown in Table 2, sample at 4 h shows an excess of oxygen compared to the other samples, due to the presence of ZnO in the ZnS thin film. Fig. 5 shows the XPS signal corresponding to O 1s, where two energies can be seen for sample at 4 h of deposition time 532.1 ± 0.1 eV and 530.5 ± 0.1 eV, attributed to Zn—OH and zinc atoms bonded to oxide atoms (Zn—O) bonds, respectively [38]. The binding energy corresponding to ZnO was not observed for films grown at longer deposition times, which could explain the excess of oxygen for sample at 4 h. Otherwise, in Table 2, a decrease in (S/O) ratio can be seen as the deposition time increases, probably because of an increase of $Zn(OH)_2$ in thin films; also, the same phenomenon can be observed in [S/Zn] ratio, due to an excess of hydroxide in the solution. G. Hodes reported that Zn^{2+} and S^{2-} ions will prefer adsorb to colloids of hydroxide in the solution over nucleation on substrate [21], situation that was also observed during the growing of the thin films reported here. When Zn^{2+} and S^{2-} ions are free in the solution, they will react minimizing the energy, and in presence of a solid phase (like metallic hydroxide) the ions will adsorb to $Zn(OH)_2$ since this process requires less energy compared to that required to form a nucleus on the substrate surface.

Table 2
The thin films relative composition in atomic percent determined by XPS software.

Time (h)	At (%)				
	O	Zn	S	(S/Zn)	(S/O)
4	63.2	30.6	6.2	0.2026	0.0981
8	25.1	60.8	14.1	0.2319	0.5617
12	26.8	60.6	12.7	0.2095	0.4738
16	25.8	63.6	10.6	0.1666	0.4108

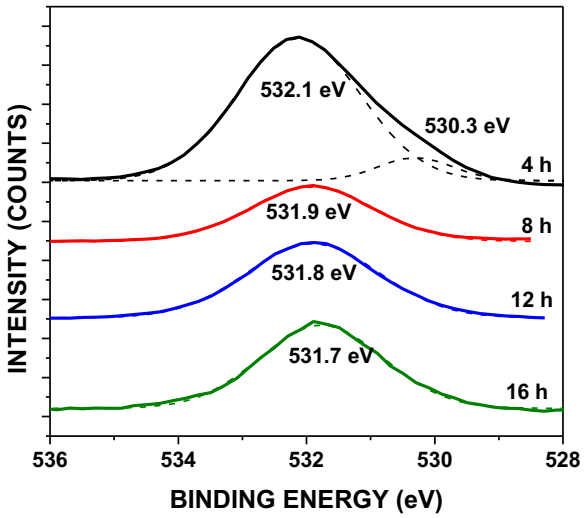

Fig. 5. O 1s XPS spectra for ZnS thin films.

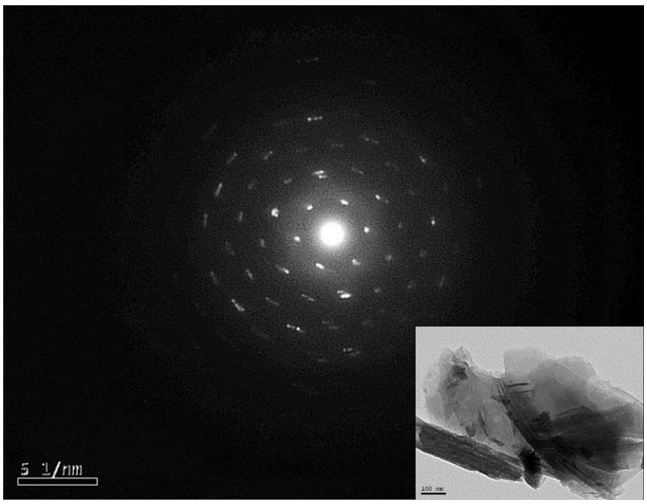

Fig. 6. Electron diffraction patterns of sample obtained from ZnS thin films grown at 4 h.

3.4. Structural analysis

Mostly, zinc sulfide exists in two structures: wurtzita-hexagonal and zinc blende-cubic. The cubic phase is stable at room temperature, while the less dense hexagonal phase is stable above 1200 °C and at atmospheric pressure. However, hexagonal structure has been reported for ZnS–CBD [37].

In order to obtain the structural information of the samples, TEM studies were done. Fig 6 shows electron diffraction-pattern images for thin film deposited at 4 h, which was carefully scraped and laid on equipment grid. In Fig. 6, the polycrystalline nature of the film is observed, exhibiting a pattern of a set of point-forming rings. Using image-editing software, it was possible to determine the interplanar distances (*d*-spacing) measuring the diameters of the rings in order to index, which were compared to the theoretical values. The calculated *d*-spacings are shown in Table 3. The *d*-spacings found were assigned to reflections of hexagonal phase planes type wurtzite-8H (PDF N°.: 72-0163). Furthermore, X-ray diffraction measurements were performed to study the crystal structure of ZnS thin films and to complement the electron diffraction studies. Since the ZnS–CBD tends to be very thin (<100 nm), the deposition was performed several times in order to obtain thicker samples. Fig. 7 shows XRD patterns of ZnS thin films deposited on glass substrate at different deposition times, which reveals the nanocrystalline nature of samples. Independently of the deposition time, X-ray diffraction patterns show a clear and low intensity peak at 2θ of approximately 29.54°, which can be assigned to the hexagonal (1 0 3) plane (PDF N°.: 72-0163) or to the cubic (1 1 1) plane (PDF N°.: 03-0524) of ZnS. Unfortunately, it is impossible to distinguish clearly into hexagonal or cubic planes because the diffraction angles for these planes are similar. Nonetheless, very low intensity peaks positioned at 2θ 46.56°, 55.45°, 58.48° and 63.20° can be appreciated, which were attributed at hexagonal planes (1 1 0), (2 0 1), (2 0 5) and (2 0 8), respectively, of the hexagonal phase (wurtzite-8H, PDF N°.:72-0163). The low intensity of diffracted peaks as well as the signal lifting of the pattern between 2θ values 20° and 40° are attributable to ZnS thin films grown preferably amorphous; this

Table 3
Interplanar spacing *h k l* of ZnS thin film deposited at 4 h.

d-spacing (Å) PDF N°.:72-0163	*d*-spacing (Å) experimental	Plane (*h k l*)
4.1600	4.5250	(0 0 6)
2.5892	2.6193	(1 0 6)
2.2698	2.2810	(1 0 8)
1.7608	1.7134	(1 0 12)
1.5600	1.5524	(0 0 16)
1.4466	1.3378	(2 0 11)
1.2441	1.2457	(2 1 2)

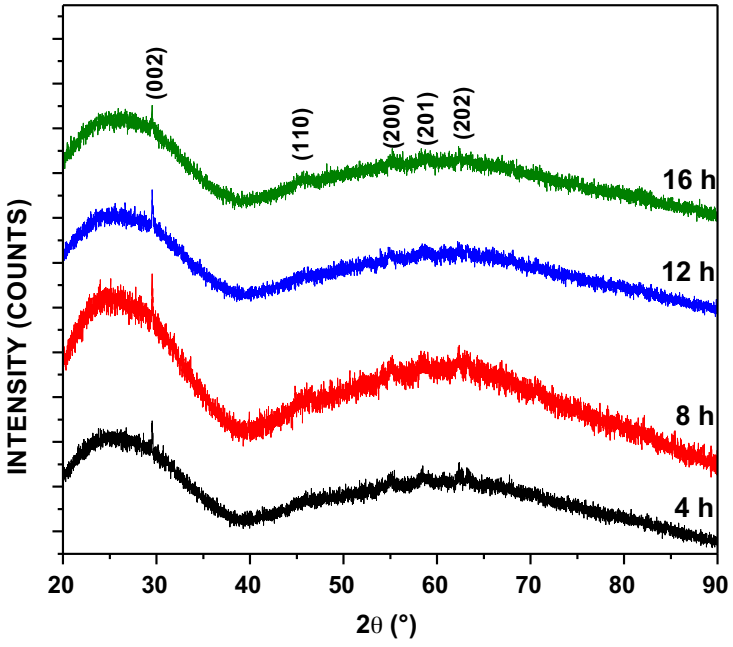

Fig. 7. XRD patterns of ZnS thin films grown at 4, 8, 12 and 16 h.

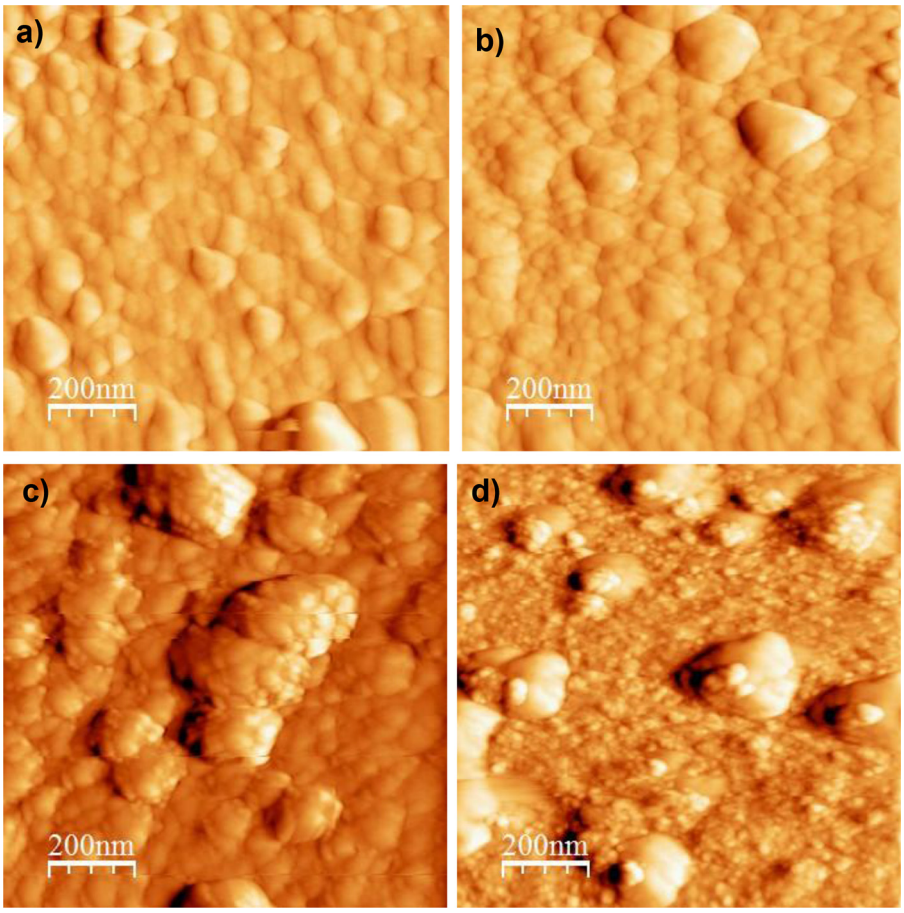

Fig. 8. Typical 1 μm^2 AFM images of ZnS thin films deposited at (a) 4, (b) 8, (c) 12 and (d) 16 h.

phenomenon has been previously reported by several authors [14,15,37]. From the crystallographic and optical properties aspect mentioned above, the thin films prepared without any flammable and volatile material is an excellent eco-friendly route to prepare high-quality ZnS thin films.

3.5. Morphological analysis

The surface characteristics of ZnS thin films were determined by means of AFM in contact mode with areas of 1 $\mu m \times 1$ μm. Fig. 8 shows 1 μm^2 AFM images of ZnS thin films on glass substrates as a function of deposition time. From that figure, it is clear that the samples are uniform, compact, and that a substrate surface well covering by fine spherical and elliptical particles was achieved. The morphological study indicates roughness values from the software built at microscope of 2.94, 5.98, 9.02 and 10.45 nm as the deposition time increased to 4, 8, 12 and 16 h, respectively. This effect is caused by a clear increase in the quantity of aggregates on the surface, which is usually attributed to the involvement of cluster-by-cluster mechanism in the films grown. If the concentration of suspended particles is sufficiently high, then the probability of collisions among them becomes high. This situation can result in aggregation or coalescence. The aggregation process gives as result large particles named "aggregates". In semiconductor thin films grown by alkaline solution controlling the metal hydroxide concentration becomes difficult to occur. Accordingly the surface morphology is characterized by the presence of aggregates.

Following the previous idea, the relatively large OH^- concentration will produce that prior to completion of the ion exchange, new particles of $Zn(OH)_2$ and Zn(OH,S) will nucleate and grow on the surface of the previous particle, avoiding the continuation of the ion exchange; consequently, the sample will have hydroxide in one way or another [21]. Furthermore, it is possible to observe a clear decrease in the particle size as the deposition time increases.

The decrease in particle size can be thoroughly studied if a major magnification is performed. As seen in Fig. 9(a) for sample at 4 h, there are few particles with size lower than 47 nm. Nevertheless, as the deposition time increases, a greater amount of particles with size lower than 47 nm is observed (Fig. 9(d)). Such tendency to decrease in particle size remains in the sample at longer deposition time, where most of them are under 40 nm. The average particle size (D) and the standard deviation (SD) was estimated using ImageJ® software [41], whose values are summarized in Table 4. Fig. 10 shows the process by which the particles size would decrease as the deposition time increased. That phenomenon can be explained considering that the growth of previous layers creates preferential nucleation sites (Fig. 10(a)) where, after the first layer is deposited, the Zn(OH,S) particles will be deposited in (Fig. 10(b)). Since these sites are void spaces among ZnS particles, the particles with lower size will be adsorbed thus minimizing energy, which will cause a decrease in the particle size deposited. Finally, considering the aggregate presence and the particle size diminution, the overall effect will be a decrease in the particle size and at the same time an increase in the aggregates amount on the film surface, as shown in AFM images.

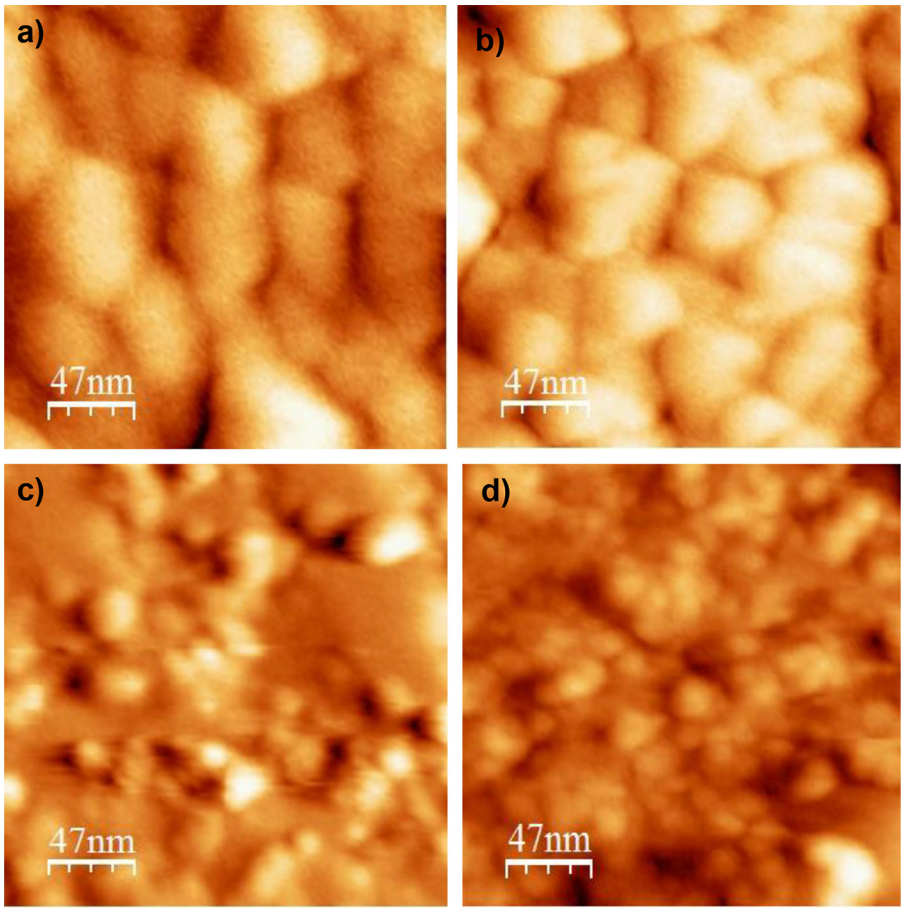

Fig. 9. Magnified AFM images for ZnS thin films deposited at (a) 4, (b) 8, (c) 12 and (d) 16 h.

Table 4
Particles size for ZnS thin films deposited at 4, 8, 12 and 16 h.

Time (h)	*D* (nm)	SD (nm)
4	48.71	19.39
8	40.64	19.18
12	29.40	16.63
16	15.89	5.30

4. Conclusions

In this work, zinc sulfide thin films grown at different deposition times through chemical bath deposition method using several times growth was performed. Deposits were carried out by means of a non-toxic alkaline solution, and the samples were translucent, homogeneous and adherent.

From optical transmission and absorption spectroscopy, it was observed that optical properties of the thin films are thickness-dependent, having a high optical transmission and band gap energy. These results indicated that ZnS thin films grown by means

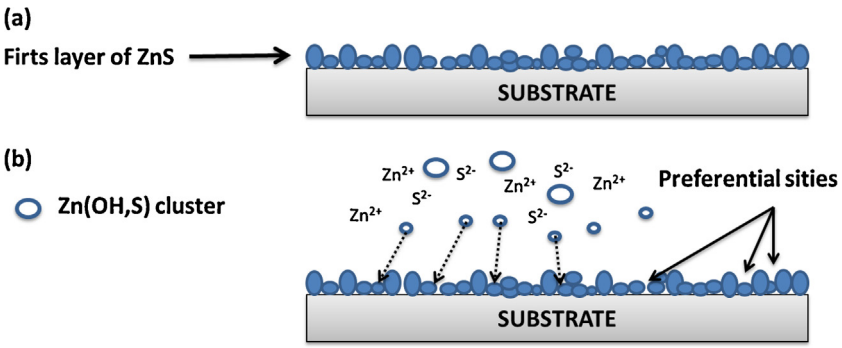

Fig. 10. Scheme of grown in several times of ZnS thin films.

of non-toxic solution are comparable to the data reported by other authors (transmittance close to 80% and band gap of 3.8 eV), and consequently, they are suitable for window layer material.

From the XPS, XRD and TEM measurements, it was concluded that thin films are a mixture of ZnS and $Zn(OH)_2$ name for some works as Zn(S,OH) thin films, where ZnS hexagonal phase was identified. However, it was possible to observe growth of thin films with amorphous structural characteristics. The $Zn(OH)_2$ suggested that the cluster-by-cluster mechanism took place in the films grown, which was subsequently confirmed by images of surface morphology of the samples from AFM measurements.

The abovementioned results established that ZnS thin films can be grown avoiding the use of toxic precursors, without affecting negatively the thin films properties. From characterization, it was evident that deposits of ZnS–CBD using a non-toxic solution are suitable as window layer for TFSC.

Acknowledgements

This work was financially supported by Project DIUC210.011.050-1.0. C.A. Rodríguez appreciates the support provided by Conicyt through Grant for Doctoral Theses N°. 21110556.

References

[1] V. Demitrova, J. Tate, Thin Solid Films 365 (1) (2000) 134.
[2] L.X. Shao, K.H. Chang, H.L. Hwang, Appl. Surf. Sci. 212–213 (2003) 305 (SPEC).
[3] M. Ichimura, F. Goto, Y. Ono, E. Arai, J. Cryst. Growth 198–199 (1999) 308 (Part I).
[4] G.L. Agawane, S. Shin, M. Kim, M. Suryawanshi, K. Gurav, A. Moholkar, J. Lee, J. Yun, P. Patil, J. Kim, Curr. Appl. Phys. 13 (2013) 850–856.
[5] P. Jackson, D. Hariskos, E. Lotter, S. Paetel, R. Wuerz, R. Menner, W. Wischmann, M. Powalla, Prog. Photovoltaics Res. Appl. 19 (2011) 894–897.
[6] T. Nakada, K. Furumi, A. Kunioka, IEEE Trans. Electron Devices 46 (1999) 2093.
[7] R. Bhattacharya, K. Ramanathan, Solar Energy 77 (2004) 679–683.
[8] T. Nakada, M. Hongo, E. Hayashi, Thin Solid Films 431–432 (2003) 242–248.
[9] S. Shin, S. Kang, J. Yun, A. Moholkar, J. Moon, J. Lee, J. Kim, Solar Energy Mater. Solar Cells 95 (2011) 856–863.
[10] M. Sandoval, M. Sotelo, J. Valenzuela, M. Flores, R. Ramírez, Thin Solid Films 472 (2005) 5–10.
[11] J. Herrero, M. Gutierrez, C. Guillén, J. Doña, M. Martínez, A. Chaparro, R. Bayón, Thin Solid Films 361–362 (2000) 28.
[12] M. Contreras, T. Nakada, M. Hongo, A. Pudov, J. Sites, ZnO/ZnS(O,OH)/Cu(In,Ga)Se_2/Mo solar cell with 18.6% efficiency, 3rd World Conference on Photovoltaic Energy Conversion May 11–18, Osaka, Japan, 2003, pp. 570.
[13] N. Allouche, T. Nasr, N. Kamoun, C. Guasch, Mater. Chem. Phys. 123 (2010) 620–624.
[14] V. Vallejo, M. Hurtado, G. Gordillo, Electrochim. Acta 55 (2010) 5610–5616.
[15] S. Shin, G.L. Agawane, M. Gang, A. Moholkar, J. Moon, J. Kim, J. Lee, J. Alloys Compd. 526 (2012) 25–30.
[16] I. Carreón, L. González, M. Pech, R. Ramírez, Thin Solid Film 548 (2013) 270–274.
[17] G. Agawane, S. Shin, A. Moholkar, K. Gurav, J. Yun, J. Lee, J. Kim, J. Alloys Compd. 535 (2012) 53–61.
[18] J. Liu, A. Wei, Y. Zhao, J. Alloys Compd. 588 (2014) 228–234.
[19] S. Kang, S. Shin, D. Choi, A. Moholkar, J. Moon, J. Kim, Curr. Appl. Phys. 10 (2010) S473–S477.
[20] I. Horcas, R. Fernandez, J. Gomez, J. Colchero, J. Gomez, A. Baro, Rev. Sci. Instrum. 78 (2007) 13705.
[21] G. Hodes, Chemical Solution Deposition of Semiconductor Films, Marcel Dekker, Inc., New York, 2002.
[22] B. Treumann, L.M. Ferris, J. Am. Chem. Soc. 80 (1958) 5050.
[23] P. Roy, J. Ota, S.K. Srivastava, Thin Solid Films 515 (2006) 1912–1917.
[24] S. Tec-Yan, J. Rojas, V. Rejón, A.I. Oliva, Mater. Chem. Phys. 136 (2012) 386–393.
[25] A. Goux, T. Pauporté, J. Chivot, D. Lincot, Electrochem. Acta 50 (2005) 2239–2248.
[26] T. Ishizaki, T. Ohomoto, Y. Sakamoto, A. Fuwa, Mater. Trans. 45 (2004) 277–280.
[27] R. Krotz, B. Evangelou, G. Wagner, Plant Physiol. 91 (1989) 780–787.
[28] A. Goudarzi, G. Aval, R. Sahraei, H. Ahmadpoor, Thin Solid Films 516 (2008) 4953–4957.
[29] S. Shin, S. Kang, K. Gurav, J. Yun, J. Moon, J. Lee, J. Kim, Solar Energy 85 (2011) 2903–2911.
[30] R. Ochoa-Landín, M. Sandoval-Paz, M. Ortuño-López, M. Sotelo-Lerma, R. Ramírez-Bom, J. Phys. Chem. Solid 70 (2009) 1034–1041.
[31] K. Nanda, S. Sahu, Adv. Mater. 13 (2001) 280–283.
[32] R. Moubah, S. Colis, M. Gallart, G. Schmerber, P. Gilliot, A. Dinia, J. Lumin. 132 (2012) 457–460.
[33] Q. Liu, J. Shi, Z. Li, D. Zhang, X. Li, Z. Sun, L. Zhang, S. Huang, Physics B 405 (2010) 4360–4365.
[34] F. Long, W. Wang, Z. Cui, L. Fan, Z. Zou, T. Jia, Chem. Phys. Lett. 462 (2008) 84–87.
[35] Z. Limei, X. Yuzhi, L. Jianfeng, J. Environ. Sci. (2009) S76–S79.
[36] F. Yakuphanoglu, M. Sekerci, A. Balaban, Opt. Mater. 27 (2005) 1369–1372.
[37] D. Johnston, M. Carletto, K. Reddy, I. Forbes, R. Miles, Thin Solid Films 403 (2002) 102.
[38] W. Eisele, A. Ennaoui, P. Schubert, M. Giersig, C. Pettenkofer, J. Karuser, M. Lux, S. Zweigar, F. Karg, Sol. Energy Mater. Solar Cells 75 (2003) 17–26.
[39] M. López, J. Espinos, F. Martín, D. Leinen, J. Ramos, J. Cryst. Growth 285 (2005) 66–75.
[40] C.D. Wagner, W.M. Ringgs, L.E. Davis, J.F. Moulder, in: G.E. Muilenberg (Ed.), Handbook of X-ray Photoelectron Spectroscopy, PerkinElmer Corporation, Minnesota, 1979.
[41] S. Bahamondes, S. Donoso, R. Henríquez, G. Kremer, R. Muñoz, M. Flores, Av. Cien. Ing. 3 (2) (2012) 79–86.